Remote Sensing of Environment 112 (2008) 3656–3667

Contents lists available at ScienceDirect

Remote Sensing of Environment

journal homepage: www.elsevier.com/locate/rse

Estimation of snow water equivalent over first-year sea ice using AMSR-E and surface observations

A. Langlois [a,*], R. Scharien [b], T. Geldsetzer [b], J. Iacozza [a], D.G. Barber [a], J. Yackel [b]

[a] Centre for Earth Observation Science (CEOS), Department of Environment and Geography, University of Manitoba, Winnipeg, Canada R3T 2N2
[b] Department of Geography, University of Calgary, Calgary, Canada T2N 1N4

ARTICLE INFO

Article history:
Received 2 November 2007
Received in revised form 23 March 2008
Accepted 24 May 2008

Keywords:
Snow water equivalent
Arctic
First-year sea ice
Passive microwaves
Surface based radiometer
AMSR-E
Ice roughness
Climate change

ABSTRACT

A SWE retrieval algorithm developed in-situ using passive microwave surface based radiometer data is applied to the Advanced Microwave Scanning Radiometer for Earth Observation System (AMSR-E). Snow water equivalent is predicted from two pixels located in Canadian Arctic Shelf Exchange Study (CASES) overwintering study area in Franklin Bay, N.W.T., Canada. Results show that the satellite SWE predictions are statistically valid with measured in-situ snow thickness data in both smooth and rough ice environments where predicted values range from 15 to 25 mm. Stronger correlation between measured and predicted data is found over smooth ice with R^2 value of 0.75 and 0.73 for both pixels respectively. Furthermore, a qualitative study of sea ice roughness using both passive and active microwave satellite data shows that the two pixels are rougher than the surrounding areas, but the SWE predictions do not seem to be affected significantly.

1. Introduction

Snow cover plays a primary role determining the thermodynamic state of the sea ice by controlling both radiative and mass transfers across the ocean-sea ice-atmosphere interface (e.g., Eiken, 2003). The surface energy balance (SEB) along with sea ice freeze-up and decay are strongly influenced by snow thickness and its thermophysical properties such as density, temperature, salinity and grain size (e.g., Langlois and Barber, 2007b). Given the recent dramatic ice depletion observed in the Arctic over the past three decades (Francis, Hunter, Key, Wang, 2005; Stroeve et al., 2005), global accurate snow measurements are required to assess the impact of the current and future changes in the Arctic environment.

Passive microwave satellite remote sensing is known as the best tool for regional snow thickness studies (Chang, Foster, Hall, 1987; Foster et al., 2005; Cordisco, Prigent, Aires, 2006) and recent results over sea ice are promising (Cavalieri and Comiso, 2004; Markus, Powell, Wang, 2006; Langlois and Barber, 2007a). Most of the satellite studies make use of a combination of 19 and 37 GHz channels to retrieve snow depth, whereas results from in-situ measurements using surface based radiometers (SBR) provide better predictions using single frequency/polarization algorithms (Barber, Iacozza, and Walker, 2003; Langlois, Barber, Hwang, 2007b).

One of the main challenges in global SWE retrieval studies over sea ice relates to spatial heterogeneity (e.g., Sturm et al., 2006). For instance, brightness temperatures from the Advanced Microwave Scanning Radiometer for Earth Observing System (AMSR-E) include emission contributions from different surface features (smooth ice, rough ice, open water) found in a pixel of 12.5×12.5 km (e.g., Mäkynen and Hallikainen, 2005) that can potentially alter SWE predictions thus, the effect of ice roughness on existing algorithms needs to be addressed.

With increasing ice roughness, the scattering increases and the polarization effect is expected to decrease (e.g., Mätzler, 1987; Eppler, 1992). Hence, the discrimination between smooth ice and ice ridges is possible due to the strong polarization effect of a layered snowpack (e.g., Garrity, 1992). Previous results from Kurvonen and Hallikainen (1997) showed good detection of deformed ice and old level ice using a combination of high (94 GHz) and low (24 or 34 GHz) frequencies airborne brightness temperature data. Furthermore, Mäkynen and Hallikainen (2005) investigated the effect of ice deformation on the passive microwaves polarization ratio (PR) and gradient ratio (GR) for different types of snow covers. Their results showed that the polarization ratio decreases with increasing ice roughness for both dry and moist snow but they had no success in discriminating all ice types. The combination of passive microwave brightness temperatures along with synthetic aperture radar (SAR) backscatter information

* Corresponding author. Centre d'Applications et de Recherches en Télédétection (CARTEL), Département de Géomatique Appliquée, Université de Sherbrooke, Sherbrooke, Québec, J1K 2R1, Local A6-2011, Canada. Tel.: +1 819 821 8000x62195; fax: +1 819 821 7944.
E-mail address: A.Langlois2@USherbrooke.ca (A. Langlois).

0034-4257/$ – see front matter
doi:10.1016/j.rse.2008.05.004

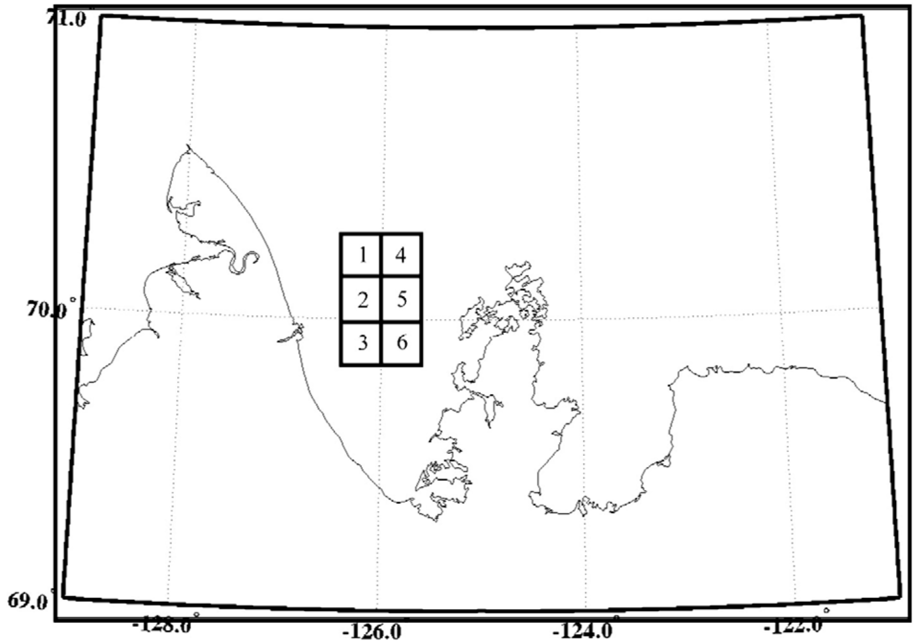

Fig. 1. AMSR-E pixel location within Franklin Bay, N.W.T.

could improve sea ice roughness information and very few studies have looked into this issue.

Therefore, the objectives of this paper are to a) apply the SWE algorithm developed from in-situ data by Langlois and Barber (2007a) to AMSR-E satellite data, b) to validate the predictions with in-situ measured snow thickness data, and c) to evaluate the effect of surface roughness on the SWE predictions using a combination of passive and active microwave data.

2. Data and methods

2.1. Study location

The study period extended between day 343 (December 7th, 2003) and 122 (April 30th, 2004) during the Canadian Arctic Shelf Exchange Study (CASES), in Franklin Bay, Northwest Territories, Canada. The Canadian Coast Guard icebreaker C.C.G.S. Amundsen was frozen into a pan of smooth ice where all the physical sampling occurred (Langlois, Mundy, Barber, 2007a). We used brightness temperatures from 6 adjacent pixels (12.5 km resolution) from AMSR-E within the bay (Fig. 1). The central coordinates of these pixels are displayed in Table 1.

2.2. Snow thickness

A series of thickness transects were conducted in different ice roughness conditions, and have been used for validation of the SWE predictions. Snow thickness lines were sampled at 0° (E–W direction), 45°, 90° (N–S direction) and 135° at a sampling interval of 1 m following a method developed by Iacozza and Barber (2001). The sampled zone for SWE transects was 50×50 m, with sampling lines varying between 50 and 71 m from the directions mentioned above. The total number of samples varied between 483 and 500 for smooth transects as it varied between 477 and 505 for rough transects. We calculated SWE for the snow thickness measurements by incorporating density profiles measured at the ship's sampling site (Langlois et al., 2007a) over the same period and thickness range. Since the ship's was located in a smooth area, most of smooth SWE transects occurred near the ship between 0.19 km and 2.05 km distance (average of 1.32 km on Table 2). Rough ice SWE transects were located at a distance varying between 1.06 km and 2.63 km (average of 1.95 km on Table 3).

2.3. AMSR-E brightness temperatures

Brightness temperatures, T_b, were extracted from AMSR-E at both 18.7 and 36.5 GHz. The sensor was launched on the National Aeronautics and Space Administration (NASA) Aqua satellite (polar/sun-synchronous orbit) in May of 2002. The sensor collects data at six frequencies (6.9, 10.7, 18.7, 36.5, and 89 GHz in both horizontal and

Table 1
Coordinates of the AMSR-E pixels

Pixel 1	70.0403 N	−125.9421 W
Pixel 2	69.9296 N	−125.9934 W
Pixel 3	69.8190 N	−126.0442 W
Pixel 4	70.0223 N	−125.6185 W
Pixel 5	69.9118 N	−125.7241 W
Pixel 6	69.8013 N	−125.7241 W

Table 2
Basic SWE statistical data calculated from smooth ice snow thickness data

ID	Day	Latitude	Longitude	Transects SWE				AMSR-E SWE	
				Min	Max	Mean	SD	p-Min	p-Max
1	21	70.033	−126.342	11.3	18.7	12.9	11.0	16.1	16.3
2	24	70.043	−126.258	11.5	27.6	15.6	13.5	15.3	15.8
3	28	70.04	−126.26	11.7	25.9	14.5	13.0	18.0	18.5
4	32	70.041	−126.255	11.8	27.4	15.6	13.8	15.9	16.2
5	40	70.048	−126.255	11.7	34.1	16.5	13.6	17.4	17.9
6	48	70.051	−126.313	11.2	28.4	14.2	13.0	16.4	16.9
7	57	70.052	−126.3	12.6	26.6	15.4	12.8	17.0	17.9
8	65	70.052	−126.302	11.0	38.0	14.9	13.5	15.6	16.0
9	71	70.042	−126.302	11.7	34.1	15.7	14.0	15.2	15.5
10	76	70.051	−126.271	12.6	37.6	16	13.9	17.4	17.5
11	80	70.056	−126.288	12.1	48.6	18.7	16.8	16.7	16.7
12	83	70.056	−126.281	12.3	39.2	16.7	14.9	16.8	17.3
13	96	70.058	−126.29	14.4	46.6	23.7	17.7	20.8	21.4
14	99	70.039	−126.254	13.0	42.7	20.5	16.4	20.9	21.6
15	101	70.045	−126.256	13.8	58.6	23.6	17.4	21.4	21.8
16	119	70.044	−126.305	10.8	42.1	21.6	17.2	21.2	21.9